

Four-wave mixing Bragg scattering for small frequency shift from silicon coupled microrings

Chang Zhao(赵畅), Chao Wu(吴超), Pingyu Zhu(朱枰谕), Yuxing Du(杜昱星), Yan Wang(王焱), Miaomiao Yu(余苗苗), Kaikai Zhang(张凯凯), and Ping Xu(徐平)

Citation: Chin. Phys. B, 2025, 34 (**1**): 014206. DOI: 10.1088/1674-1056/ad8a4f
Journal homepage: http://cpb.iphy.ac.cn; http://iopscience.iop.org/cpb

What follows is a list of articles you may be interested in

Intrinsic polarization conversion and avoided-mode crossing in X-cut lithium niobate microrings

Zelin Tan(谭泽林), Jianfa Zhang(张检发), Zhihong Zhu(朱志宏), Wei Chen(陈伟), Zhengzheng Shao(邵铮铮), Ken Liu(刘肯), and Shiqiao Qin(秦石乔)
Chin. Phys. B, 2024, 33 (**6**): 064205. DOI: 10.1088/1674-1056/ad47b2

Effects of cross-Kerr coupling on transmission spectrum of double-cavity optomechanical system

Li-Teng Chen(陈立滕), Li-Guo Qin(秦立国), Li-Jun Tian(田立君), Jie-Hui Huang(黄接辉), Nan-Run Zhou(周南润), and Shang-Qing Gong(龚尚庆)
Chin. Phys. B, 2024, 33 (**6**): 064204. DOI: 10.1088/1674-1056/ad2507

Effectively modulating spatial vortex four-wave mixing in a diamond atomic system

Nuo Ba(巴诺), Ming-Qi Jiang(姜明奇), Jin-You Fei(费金友), Dan Wang(王丹), Hai-Lin Jiang(蒋海林), Lei Wang(王磊), and Hai-Hua Wang(王海华)
Chin. Phys. B, 2024, 33 (**4**): 044202. DOI: 10.1088/1674-1056/ad0771

Generation of spectrally uncorrelated biphotons via fiber nonlinear quantum interference

Zhengtong Wei(卫正统), Chuan Qu(瞿川), Tian'an Wu(吴天安), Yuanyuan Li(李媛媛), Bo Li(李博), and Shenghai Zhang(张胜海)
Chin. Phys. B, 2023, 32 (**6**): 064202. DOI: 10.1088/1674-1056/acb767

Absorption spectra and enhanced Kerr nonlinearity in a four-level system

Hao-Jie Huangfu(皇甫浩杰), Ying-Jie Du(杜英杰), and Ai-Hua Gao(高爱华)
Chin. Phys. B, 2023, 32 (**11**): 114214. DOI: 10.1088/1674-1056/ad0622

Four-wave mixing Bragg scattering for small frequency shift from silicon coupled microrings

Chang Zhao(赵畅), Chao Wu(吴超), Pingyu Zhu(朱枰谕), Yuxing Du(杜昱星), Yan Wang(王焱), Miaomiao Yu(余苗苗), Kaikai Zhang(张凯凯), and Ping Xu(徐平)†

Institute for Quantum Information & State Key Laboratory of High Performance Computing, College of Computer Science and Technology, National University of Defense Technology, Changsha 410073, *China*

(Received 26 September 2024; revised manuscript received 17 October 2024; accepted manuscript online 23 October 2024)

Frequency conversion is pivotal in nonlinear optics and quantum optics for manipulating and translating light signals across different wavelength regimes. Achieving frequency conversion between two light beams with a small frequency interval is a central challenge. In this work, we design a pair of coupled silicon microrings wherein coupled-induced mode-splitting exists to achieve a small frequency shift by the process of four-wave mixing Bragg scattering. As an example, the signal can be up or down converted to the idler which is 15.5 GHz spaced when two pumps align with another pair of split resonances. The results unveil the potential of coupled microring resonators for small interval frequency conversion in a high-fidelity, all-optical, and signal processing quantum frequency interface.

Keywords: four-wave mixing, Bragg scattering, silicon coupled microrings

PACS: 42.65.Wi, 42.65.–k, 42.82.–m, 42.82.Et

DOI: 10.1088/1674-1056/ad8a4f **CSTR:** 32038.14.CPB.ad8a4f

1. Introduction

Nonlinear optical frequency conversion leverages the nonlinear interactions between light and matter to effectively convert the frequency of optical signals, which holds significant importance for advancing the fields of optical communication,[1] quantum information science,[2] and photonic integrated circuits.[3] It is particularly worth noting that frequency conversion between two closely spaced wavelengths is of great value, enabling a range of applications, such as high-density optical signal encoding and processing,[5] and facilitating single-photon frequency conversion and logical operations, including frequency-based single-photon Hong–Ou–Mandel (HOM) interference[6] and controlled-NOT (CNOT).[7]

Currently, various second-order and third-order nonlinear materials can achieve frequency conversion with small wavelength intervals. This can be accomplished through the difference frequency generation in second-order nonlinear crystals[8] or by electro-optic modulation in lithium niobate for minor frequency shifts.[9,10] In this context, we propose to use silicon photonic chips because silicon on insulator (SOI) platforms offer compatibility with complementary metal oxide semiconductor (CMOS) processes, exhibit high nonlinear coefficients, and possess high refractive indices. These characteristics render SOI an ideal platform for all-optical signal processing and developing large-scale optical quantum information processing applications.[11–14]

In the four-wave mixing (FWM) process governed by the energy conservation of $w_i = 2w_p - w_s$, the signal and idler beams are symmetrically situated on either side of the pump. However, to achieve small interval frequency conversion, the signal and idler are so close to the pump that the filtering of the strong pump is extremely difficult. To deal with this issue, we can employ four-wave mixing Bragg scattering (FWM-BS),[15–17] wherein the signal beam or single-photon state can be coherently transferred to a new frequency, which is determined by the frequency difference between the two pump beams. The energy conservation FWM-BS satisfies $w_i = w_s \pm (w_{p1} - w_{p2})$. The FWM-BS process can be visualized as the interference of the two pump beams effectively creating a grating within the nonlinear medium, which scatters the signal into two idlers. Since the pump beams can be far from the signal and idler beams, the pump is greatly restrained when detecting the converted idler beams.

Microring resonators are widely used in experiments to implement FWM owing to their ability to significantly enhance the field strength, thus achieving more efficient frequency conversion within a smaller mode volume. In this work, by implementing FWM-BS in the microring, we choose the resonance of pump, signal, and idler, where the pump is far away from the signal and idler, thereby decreasing the impact of the residual pump on the converted beams. By fine-aligning the resonances and coupling two microrings with identical circumference, we induce coupled mode-splitting for every resonance. We use a single pulsed pump whose linewidth is larger than the interval of the split modes. When the pump aligns with one resonance, consisting of a pair of split modes, two

†Corresponding author. E-mail: pingxu520@nju.edu.cn

© 2025 Chinese Physical Society and IOP Publishing Ltd. All rights, including for text and data mining, AI training, and similar technologies, are reserved.

pump beams corresponding to two splitting modes are prepared. The signal, belonging to one of the split modes from another resonance which is one or two free spectral ranges (FSRs) away from the pump, can be scattered to the other splitting mode. For example, by implementing this strategy, a small frequency shift of 15.5 GHz, corresponding to the mode-splitting, is observed.

The rest of the paper is structured as follows. We first theoretically propose a frequency matching strategy for wavelength generation via the FWM-BS process in microring resonators. Then, we experimentally validate the proposal by situating two pumping wavelengths one and two FSRs away from the signal, and detect the presence of idler in two experimental sets with different parameters. Finally, we conclude and envision the potential applications of the proposed FWM-BS.

2. Device design and theoretical method

In this section, we introduce a new frequency matching strategy for wavelength generation via the FWM-BS process in microring resonators. Figure 1(a) shows our resonator-based frequency conversion design, which allows us to manipulate the splitting of the pump signal and idler. The rings μR_1 and μR_2 are coupled to each other directly, and each of the resonators is coupled with an asymmetric Mach–Zehnder interferometers (AMZI). Being a cavity, the ring will only support specific wavelengths of light meeting the resonant condition $2\pi R n_{\text{eff}} = m\lambda$, $m = 0, \pm1, \pm2, \ldots$, whose resonant frequencies are separated by the FSR, $\omega_{\text{FSR}} = V_g/R$, where R is radius of the ring resonator and n_{eff} is the wavelength dependent effective refractive index. The radius of the two rings is 56 μm with the waveguide's cross-section height and width being 220 nm and 500 nm, respectively. The narrowest gap between the rings is 258 nm, while the narrowest gap between the ring and AMZI is 228 nm. The path difference between AMZI's two paths is equal to the ring's round-trip length, with the thermo-optic phase shifter integrated on the waveguide of AMZI's long arm. A phase shifter also tunes the ring's resonance to align the resonant wavelength with the channel of dense wavelength division multiplexing (DWDM). A theoretical model for coupled resonators is proposed in Ref. [25]. Here each of the resonators μR_1 and μR_2 was coupled to an AMZI. We first applied voltages to the thermo-optic phase shifters on the microrings to shift their resonant wavelengths, we can distinctly observe their independent transmission spectra, each exhibiting no mode splitting. The two microring resonators have an identical radius of 56 μm, resulting in a FSR of 1.6 μm. Then, we change the voltage of the thermo-optic phase shifters on the rings, achieving frequency resonance between the two microrings, by fine tuning the voltage of the thermo-optic phase shifters on the AMZIs, the whole system completes the transition from the non-coupled to weak-coupling regime. In Fig. 1(b) we give the transmission spectra of the whole resonator system, where the two rings are in weak-coupling regime. In Fig. 1(d) we measure the transmission spectra of the coupling microrings system by scanning a tunable continuous-wave (CW) laser and recording the transmitted power with a power meter, the experimental result is in good agreement with the theoretical simulation in Fig. 1(c).

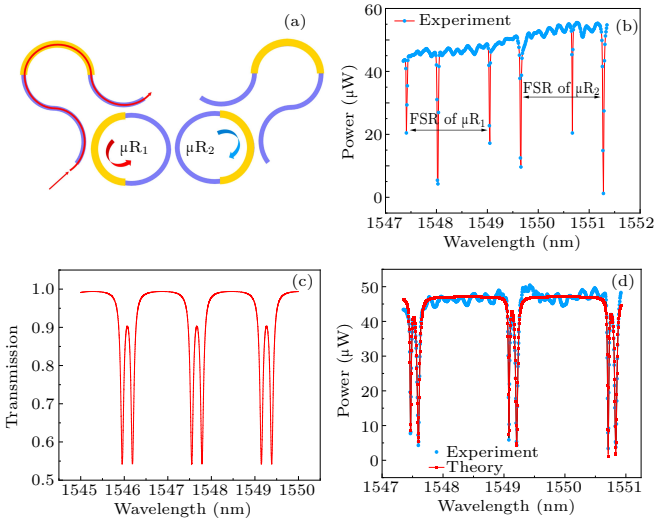


Fig. 1. (a) Schematic diagram of the coupled microrings used in our experiment, where the left ring is labeled as μR_1 and the right ring is labeled as μR_2. (b) Transmission spectrum composed of independent resonance peaks from two microring resonators. Each microring's resonance peaks are distinct and show no splitting. (c) Illustrates the simulated spectrum showing the splitting of resonance peaks due to the coupling of two microring resonators. (d) The blue dots and the red solid line represent the measured data and the theoretical fitting curve, respectively.

Figure 2 presents a schematic representation of the FWM-BS process. The pump, signal, and idler are designated as p, s, and i. Here, ω_{p1}, ω_{p2}, ω'_{p1}, ω'_{p2}, ω_{s}, and ω_{i} are their corresponding resonant frequencies. When the pump aligns with one resonance, consisting of a pair of split modes, two pump beams corresponding to two splitting modes (ω_{p1}, ω_{p2} or ω'_{p1}, ω'_{p2}) are prepared. We regard the splitting modes as pump beams, while the other splitting mode of the resonance away from the pump beams one or two FSRs was selected to observe the frequency conversion of the coupled resonators.

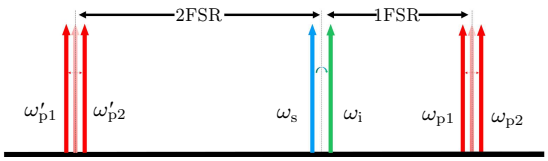


Fig. 2. Schematic diagram of FWM-BS and mode splitting.

3. Experimental results

In this section, we experimentally validate the aforementioned FWM-BS proposal in a SOI platform. Our experimental setup is shown in Fig. 3. One pulsed laser with a linewidth

of 0.15 nm served as the pump and one CW laser with full width at half maximum (FWHM) of 400 kHz served as the signal, then the lasers were controlled by two separate polarization controllers (PC) to optimize coupling efficiency between the fiber arrays and gratings on the chip. The pump was coupled by a 99:1 coupler, where the port with the 99% ratio is connected to the input port of the DWDM. The pump, signal, and the converted beams are coupled into and out of the chip using the same fiber array and a 200 GHz DWDM. The total coupling loss of coupling into and out of the chip is measured to be 11.5 dB. The other output port of the 99:1 coupler is connected to a power meter to monitor the power of the pump and signal before the chip. The converted idler alongside with residual pump and signal is also coupled out of the chip through vertical coupling between on-chip gratings and off-chip fiber arrays, a narrowband filter then separates the idler for measurement. The corresponding FWHMs of the tunable narrowband filters for the two splitting modes were 0.2 nm and 0.21 nm, respectively. By fitting the spectrum with a Lorentzian lineshape, we determined the FWHMs of the two splitting modes to be 0.02 nm and 0.027 nm, respectively. The narrowband filters fully covered the FWHM of the idler in the experiment, ensuring that the peak adjacent to the signal is the idler generated by FWM-BS. When scanning signal wavelengths across the resonant spectrum, the converted idlers are measured by an OSA instead of a power meter. A set of programmable DC power sources is connected to the chip, providing proper voltages for the phase shifters with a precision of 0.01 V. The crosstalk between the AMZIs' and the ring's heaters exists. Here, one or two rounds of back-and-forth tuning are required and sufficient.

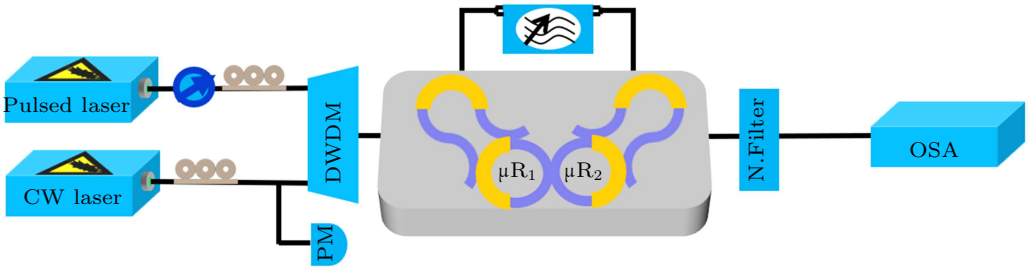


Fig. 3. Experimental setup for FWM-BS. PM, power meter; OSA, optical spectrum analyzer; DWDM, dense wavelength-division multiplexing; N.Filter, narrowband filter. In our experiments, the central wavelengths of the pump beams were specifically tuned to 1549.25 nm and 1544.4 nm, while the central wavelength of the signal aligned with one of the splitting modes away from the pump beams one or twice FSR. The variation between the signal and the idler was detected by the OSA.

In the experimental procedure, we initially ensured precise alignment of the resonance peaks of the two microring resonators, achieving uniformity in their resonant frequencies. Subsequently, by meticulously adjusting the AMZIs, we effectively induced the splitting effect of the resonance peaks. Building upon this foundation, we conducted two meticulously designed experiments, as illustrated in Fig. 4. The power values are expressed in mW rather than dB to provide a more direct representation of the power scaling. This linear scale representation effectively reduces the apparent scatter of the data points, offering a clearer visualization of the FWM-BS progress. In the first set of experiments, we finely tuned the central wavelength of the pump to 1549.25 nm with a bandwidth covering the splitting modes, precisely matching the 35th channel of the DWDM system. Furthermore, to align with the 37th channel of the DWDM system, we introduced signals at wavelengths of 1547.568 nm and 1547.692 nm. Both wavelengths of the signal were perfectly aligned with the corresponding channels of the DWDM system. The data results are shown in Figs. 4(a) and 4(b). After these beams passed through our chip and were filtered by a tunable filter, we clearly observed the spectral characteristics of the signal and idler on the OSA.

In the second set of experiments, we made adjustments based on the previous group, altering the position of the pump to move it further away from the location where the idler is generated through FWM-BS. The obtained experimental results are summarized in Figs. 5(c) and 5(d). Specifically, the central wavelength of the pump was separated from the position of the idler by the distance of two free spectral ranges. We selected a pulsed beam with a central wavelength of 1544.4 nm as the pump beam to cover the splitting modes, which precisely corresponds to the CH41 of the DWDM system. Concurrently, we continued to employ signal at wavelengths of 1547.568 nm and 1547.692 nm. After these beams passed through our chip and were filtered by a tunable filter, we were able to simultaneously observe the spectral characteristics of both the signal and converted idler on the OSA.

We characterized the power scaling of the generated idler as a function of incident pump power. The theoretical framework for this relationship has been rigorously derived in Refs. [26,27]. As illustrated in our experimental setup in Fig. 3, before entering the chip, the optical signal passed through a 99:1 splitter; however, the actual measured splitting ratio was closer to 60:1. Due to the maximum optical power that the microring resonator can tolerate, and in order to en-

sure significant idler generation, we limited the pump power to a maximum of 10 mW in our experiment. We measured the power at the 1% port and recorded 10 data points: 60 μW, 90 μW, 100 μW, 110 μW, 120 μW, 130 μW, 140 μW, 150 μW, 160 μW, and 170 μW. Simultaneously, we recorded the peak power of the idler generated via FWM-BS using an optical spectrum analyzer. We plotted the variation of the converted idlers' power as a function of the pump power (as shown in Fig. 5). It is evident that the power of the generated idler exhibits a quadratic dependence on the pump power.

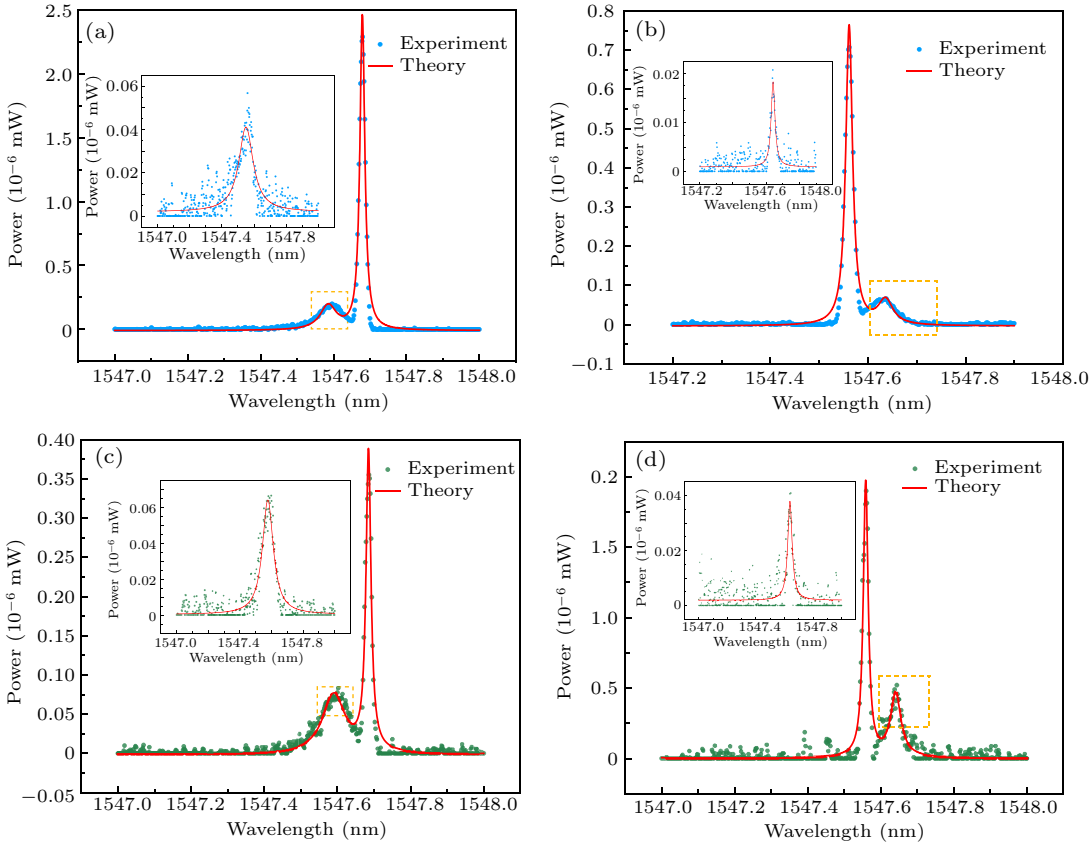


Fig. 4. The measured outcomes from two experimental sets alongside the theoretical predictions. The blue dots represent the experimental data from the first set of experiments, while the green dots denote the experimental data from the second set. The red solid lines indicate the theoretical fitting results. (a) and (b) The pulsed pump at 1549.25 nm was tuned to match the DWDM system's CH35. Continuous-wave seeds at 1547.568 nm and 1547.692 nm (one FSR away from the pump beams) were aligned with the CH37. (c) and (d) The pulsed pump at 1544.4 nm was tuned to match the DWDM system's CH41. Continuous-wave seeds at 1547.568 nm and 1547.692 nm (two FSRs away from the pump beams) were aligned with the CH37.

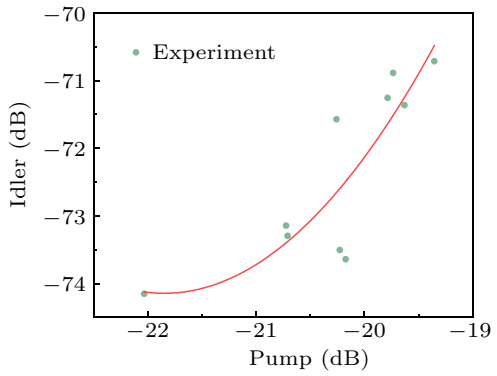


Fig. 5. The experimental data obtained from the OSA, denoted by green points, alongside the fitting results, represented by red lines.

4. Conclusions

In this paper, we have demonstrated the fine control over the coupling state of microring resonators. We achieved approximately 0.124 nm (15.5 GHz) of frequency conversion by positioning the signal at one and two FSRs (1.6 nm and 3.2 nm) from the pump wavelength. Due to the resonant splitting nature of the coupled microrings, we are able to achieve frequency conversion between closely separated frequencies. This work paves the way for the development of versatile photonic devices with elaborate spectral manipulation capabilities, holding great promise for applications in optical communication and quantum information processing.

Acknowledgement

Project supported by the National Key Research and Development Program of China (Grant No. 2022YFF0712800).

References

[1] Krupa K, Tonello A, Kozlov V V, Couderc V, Di B P, Wabnitz S, Barthélémy A, Labonté L and Tanzilli Sé 2012 *Opt. Express* **20** 27220

[2] Bennett, Charles H and DiVincenzo D P 2000 *Nature* **404** 247

[3] Nagarajan R, Joyner C H, Schneider R P, *et al.* 2005 *IEEE Journal of Selected Topics in Quantum Electronics* **11** 50

[4] Dong P, Chen Y K, Duan G H and Neilson D T 2014 *Nanophotonics* **3** 215

[5] Ouyang X, Xu Y, Xian M C, Feng Z W, Zhu L W, Cao Y Y, Lan S, Guan B O, Qiu C W, Gu M, *et al.* 2021 *Nat. Photon.* **15** 901

[6] Joshi C, Farsi A, Dutt A, Kim B Y, Ji X C, Zhao Y, Bishop A M, Lipson M and Gaeta A L 2020 *Phys. Rev. Lett.* **124** 143601

[7] Lu H H, Lukens J M, Williams B P, Imany P, Peters N A, Weiner A M and Lougovski P 2019 *npj Quantum Information* **5** 24

[8] Wang J, Sun J Q, Luo C H and Sun Q Z 2005 *Opt. Express* **13** 7405

[9] Hu Y W, Zhu D, Lu S Y, Zhu X R, Song Y X, Renaud D, Assumpcao D, Cheng R, Xin C J, Yeh M, *et al.* 2024 arXiv preprint 2404.06398

[10] Vazimali M G and Fathpour S 2022 *Adv. Photon.* **4** 034001

[11] Wang J W, Sciarrino F, Laing A and Thompson M G 2020 *Nat. Photon.* **14** 273

[12] Feng L T, Zhang M, Wang J W, Zhou X Q, Qiang X G, Guo G C and Ren X F 2022 *Photon. Res.* **10** A135

[13] Pelucchi E, Fagas G, Aharonovich I, Englund D, Figueroa E, Gong Q H, Hannes Hü, Liu J, Lu C Y, Matsuda N, *et al.* 2022 *Nat. Rev. Phys.* **4** 194

[14] Giordani T, Hoch F, Carvacho G, Spagnolo N and Sciarrino F 2023 *La Rivista del Nuovo Cimento* **46** 71

[15] Uesaka K, Wong K Y, Marhic M E and Kazovsky L G 2002 *IEEE Journal of Selected Topics in Quantum Electronics* **8** 560

[16] Marhic M E, Park Y, Yang F S and Kazovsky L G 1996 *Opt. Lett.* **21** 1906

[17] Singh A, Li Q, Liu S F, Yu Y, Lu X Y, Schneider C, Höfling S, Lawall J, Verma V, Mirin R, *et al.* 2019 *Optica* **6** 563

[18] Li A and Bogaerts W 2018 *Photon. Res.* **6** 620

[19] Li A and Bogaerts W 2019 *Laser & Photonics Reviews* **13** 1800244

[20] Li A, Huang Q S and Bogaerts W 2016 *Photon. Res.* **4** 84

[21] Li A and Bogaerts W 2017 *Opt. Express* **25** 2092

[22] McGarvey-Lechable K and Bianucci P 2018 *Phys. Rev. B* **97** 214204

[23] Dutt A, Lin Q, Yuan L Q, Minkov M, Xiao M and Fan S H 2020 *Science* **367** 59

[24] Lu X Y, Rao A, Moille G, Westly D A and Srinivasan K 2020 *Photon. Res.* **8** 1676

[25] Peng B, Özdemir, ŞK, Rotter S, Yilmaz H, Liertzer M, Monifi F, Bender CM, Nori F and Yang L 2014 *Science* **346** 328

[26] Wu C, Liu Y W, Wang Y, Ding J F, Zhu P Y, Xue S C, Yu X Y, Zheng Q L, Yu M M, Huang A Q, *et al.* 2022 *Opt. Express* **30** 9992

[27] Wu C, Liu Y W, Wang Y, Gu X W, Xue S C, Yu X X, Kong Y C, Qiang X G, Wu J J, Zhu Z H and Xu P 2019 *Chin. Phys. B* **28** 104211